Inter*net* Electronic Journal of Molecular Design

September 2002, Volume 1, Number 9, Pages 450–461

Editor: Ovidiu Ivanciuc

Special issue dedicated to Professor Haruo Hosoya on the occasion of the 65th birthday
Part 1

Guest Editor: Jun–ichi Aihara

Calculation of the Tunneling Splittings in Water Trimer with a Genetic Algorithm

Michihiko Sugawara, Hiromi Nakanishi, and Satoshi Yabushita

Department of Fundamental Science and Technology, Graduate School of Science and Technology, Keio University, 3-14-1 Hiyoshi, Kohoku-ku, Yokohama 223-8522, Japan

Received: August 20, 2002; Accepted: September 5, 2002; Published: September 30, 2002

Citation of the article:
M. Sugawara, H. Nakanishi, and S. Yabushita, Calculation of the Tunneling Splitting in Water Trimer with a Genetic Algorithm, *Internet Electron. J. Mol. Des.* **2002**, *1*, 450–461, http://www.biochempress.com.

Inter*net* Electronic Journal of Molecular Design

BioChem Press
http://www.biochempress.com

Calculation of the Tunneling Splittings in Water Trimer with a Genetic Algorithm[#]

Michihiko Sugawara,* Hiromi Nakanishi, and Satoshi Yabushita

Department of Fundamental Science and Technology, Graduate School of Science and Technology, Keio University, 3-14-1 Hiyoshi, Kohoku-ku, Yokohama 223-8522, Japan

Received: August 20, 2002; Accepted: September 5, 2002; Published: September 30, 2002

Internet Electron. J. Mol. Des. **2002**, *1* (9), 450–461

Abstract

Motivation. Although inter–molecular interaction in water cluster has been a subject of significant interest for many years, there have been very few of fully quantum mechanical studies because of the numerical difficulties associated with the multi–dimensional Schrödinger equation. In this study, vibrational eigenstates/eigenenergies with respect to three–dimensional hydrogen flipping motion in the water trimer (WT) are solved by utilizing a hybrid micro genetic algorithm (μ–GA).

Method. Hybrid μ–GA is employed to solve the Schrödinger equation, in which the conventional variational calculation is combined at the final stage to overcome the μ–GA's disadvantage, namely the slow convergence to the exact solution.

Results. Eigenstates and eigenvalues calculated by hybrid μ–GA are found to be in good agreement with the ones obtained by the discrete variable method. From the eigenvalue differences, tunneling time associated with the flipping motion of WT is evaluated to be 1.2 ns.

Conclusions. Hybrid μ–GA together with the stochastically defined fitness score makes it possible to calculate efficiently the three–dimensional vibrational eigenenergies/eigenstates of the hydrogen flipping motion in WT.

Keywords. Water trimer; micro genetic algorithm; flipping motion; tunneling splitting.

Abbreviations and notations

μ–GA, micro genetic algorithm
EPEN, empirical potential using electrons and nuclei
WT, water trimer

1 INTRODUCTION

Microscopic understanding of the intermolecular interactions in the water cluster is significantly important, since it is closely related to the chemical property of the water as a universal solvent [1–12]. On the other hand, far-infrared spectroscopy data have brought new insight into the low-frequency vibrational excitations of the water trimer (WT) [13–16]. The spectra lines observed in the region 40–90 cm^{-1} are experimentally assigned to the large–amplitude flipping motion of the free O–H bonds. For quantitative theoretical analysis of such spectral structures, fully-quantum

[#] Dedicated to Professor Haruo Hosoya on the occasion of the 65th birthday.

* Correspondence author; phone: 81-45-566-1710; fax: 81-45-566-1697; E-mail: michi@chem.keio.ac.jp.

mechanical calculation is expected. However, despite of recent development of the computer technology, quantum calculation of the *M*–dimensional (especially for $M > 3$) quantum system still remains to be a difficult problem. The conventional basis set expansion method rapidly becomes unfeasible as dimensionality increases. Moreover, for the system such as WT, in which the exchange tunneling is present, one cannot resort to approximation techniques for reducing the dimension, such as self-consistent field method based on the adiabatic approximation. Because of such difficulties, there exist very few full-quantum calculations with respect to the water clusters [5,6,9–11]. Since the discrete variable representation (DVR) is essentially one of the variant of orthodox basis function expansion methods, it still suffers from the severe increase of the basis functions with respect to the system dimension, which makes its application to *N*–water clusters difficult. The alternative stochastic method based on the Monte Carlo sampling can avoid such crucial difficulty originating from the multi-dimensionality by introducing the idea of "importance sampling" [6,11]. However, the conventional diffusion Monte Carlo method is restricted to the ground state calculation. The projector Monte Carlo method, which can take the excitation process into account, is still lacking in the capability of handling the excited state wave functions directly.

In this study, we utilize the hybrid genetic algorithm to calculate the eigenstates of the flipping motion of WT quantum mechanically, which possesses both advantages of stochastic and deterministic variational calculations. We employ the micro–GA (μ–GA) [17] for searching the optimal placing and shaping of the basis functions in the multi–dimensional coordinate space. The exact final solution is obtained by the variational calculation using the basis functions optimized by the μ–GA, which makes it possible to reduce the number of basis functions drastically.

2 CALCULATION METHODS

2.1 Micro Genetic Algorithm

In this section, we briefly summarize the μ–GA's procedure. Shown in Figure 1 is the algorithm of μ–GA schematically expressed as a flow–chart. First, all the parameters subject to the optimization are coded as a "GA–string", since the μ–GA works on a coding of the variables. In this study, we employ the conventional binary coding, in which a set of real parameter values are represented as a binary bit–string (see Step 0 in Figure 1). The initial population is prepared as randomly created bit–strings, while the population size is set adequately depending on the number of unknown parameters or the bit–length of GA–string. Each string in the population corresponds to the solution candidate. Next, the population proceeds to the evaluation and selection stage. All the strings in the population are evaluated by calculating the fitness score, which is defined so as to represent how much the string is fit to the current objective. During the evaluation procedure, the GA–strings are converted to the corresponding real parameter values.

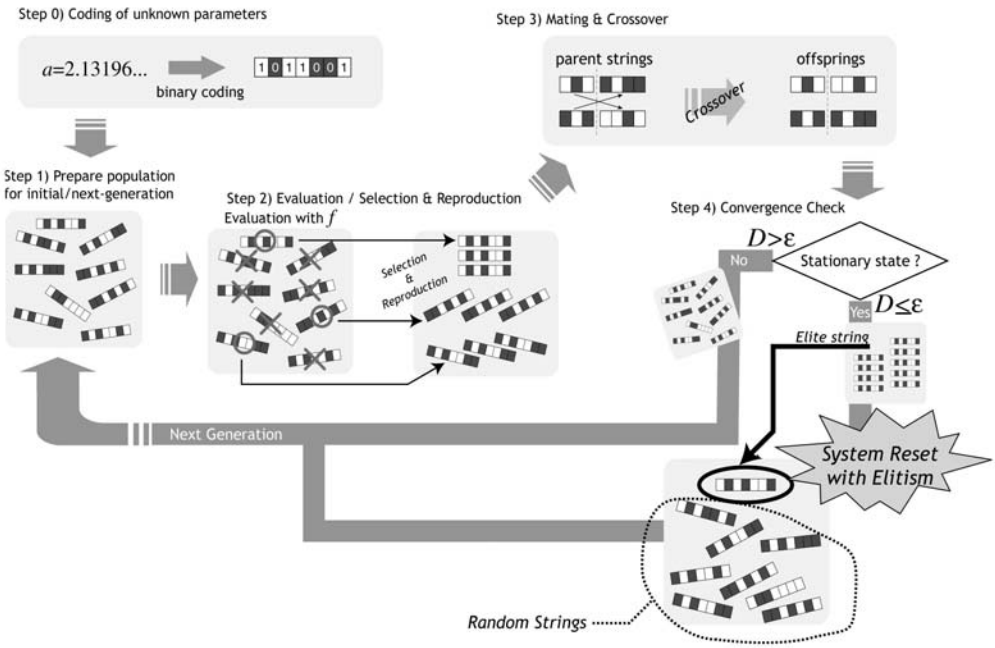

Figure 1. Schematic flow–chart of the micro–genetic algorithm.

In order to simulate the selection process we utilize the tournament selection strategy, in which a pair of strings is randomly selected from the population and the one with higher fitness is kept for the next generation. Such one–to–one competition is repeated until sufficient numbers of the strings are collected for the next generation. Next, the population is updated through mating and crossover operations. We employ the uniform crossover, in which multiple crossing points are utilized as follows. Consider parent strings p_a and p_b:

$$p_a = (a_1, \cdots, a_i, a_{i+1}, \cdots, a_j, a_{j+1}, \cdots, a_N) \tag{1}$$

$$p_b = (b_1, \cdots, b_i, b_{i+1}, \cdots, b_j, b_{j+1}, \cdots, b_N) \tag{2}$$

where a_i and b_i represent binary digits. Two offsprings o_1 and o_2 are given as

$$o_1 = (a_1, \cdots, a_i, b_{i+1}, \cdots, b_j, a_{j+1}, \cdots, a_N) \tag{3}$$

$$o_2 = (b_1, \cdots, b_i, a_{i+1}, \cdots, a_j, b_{j+1}, \cdots, b_N) \tag{4}$$

The number of the crossing points and their positions (i, j, …) are randomly determined. Convergence check is carried out as a final step at every generation. The measure of the population convergence D is defined as average bit differences between the best string among the population and other strings. If the population still evolves, or D is larger than the threshold value ε, μ–GA breeding proceeds to the next generation. If the μ–GA population reaches to the stationary state, i.e., $D < \varepsilon$, the population is reset with the randomly initialized bit–strings, leaving the best string from the previous generation.

2.2 Application to Quantum Calculation

In this section, we consider the application of μ–GA to the quantum mechanical calculation. Here, we aim to solve the stationary state Schrödinger equation given as

$$\hat{H}\,\Psi(\mathbf{x}) = E\,\Psi(\mathbf{x}) \tag{5}$$

Here, $\hat{H}$ and E denote the system Hamiltonian and the eigenvalue, respectively, whereas $\mathbf{x}$ = (x_1, x_2, …x_M) is a set of coordinate variables for M–dimensional quantum system. Under the Cartesian coordinate representation, $\hat{H}$ is given as

$$\hat{H} = -\frac{\hbar^2}{2m}\nabla^2 + V(\mathbf{x}) \tag{6}$$

where m and $V(\mathbf{x})$ are mass of a particle and the potential function. In order to solve the Schrödinger equation by μ–GA, we introduce the fitness score f defined as

$$f = \exp\left[-\frac{\int d\mathbf{x}\Psi(\mathbf{x})\left(\hat{H}-E\right)^2\Psi(\mathbf{x})}{\int d\mathbf{x}\left|\Psi(\mathbf{x})\right|^2} \right] \tag{7}$$

It is readily seen that f gives the maximum value, unity, when $\Psi(\mathbf{x})$ and E coincide with the eigenfunction and the corresponding eigenvalue, respectively. Thus, solving the Schrödinger equation turns out to be the maximization problem of the fitness score f. However, carrying out the numerical evaluation of f with respect to all the GA–strings in the population is quite a burdensome task because of the multi–dimensional integrations in Eq. (7). In order to surmount such difficulty, we reduce the computational load by introducing a new fitness score defined as

$$\tilde{f} = \exp\left[-\frac{\sum_l \left|\left(\hat{H}-E\right)\Psi(\mathbf{x}_l)\right|^2}{\sum_l \left|\Psi(\mathbf{x}_l)\right|^2} \right] \tag{8}$$

Here, $\mathbf{x}_l$ denotes the evaluation point, which is randomly distributed over the coordinate space. The evaluation point set $\{\mathbf{x}_l\}$ is renewed at every generation while the common set is used for the fitness evaluation for the strings belonging to the same generation. The effects of using the stochastically defined fitness score such as Eq. (8) on the evolution profile and overall convergence are discussed in Ref. [18].

In this study, we adopt the trial function expressed as a linear combination of M–dimensional Gaussian functions given as

$$\Psi(\mathbf{x}) = \sum_i^N c_i \prod_j^M \exp\left[-a_{ji}\left(x_j - r_{ji}\right)^2 \right] \tag{9}$$

Here, N is the number of Gaussian functions, while c_i, r_i, and a_i denote center position, width parameter and expansion coefficient of the i–th Gaussian basis function, respectively. Using μ–GA,

we seek the optimal parameter values for c_i, r_i, and a_i together with the eigenvalue E that maximize the fitness score given as Eq. (8).

It is well known that the major drawback of GA is its slow convergence to the exact optimal values. We consider the hybridization with the deterministic optimization method in order to avoid the inefficient final search by the μ–GA. After the GA–breeding with appropriate generations, we apply the conventional variational calculation. The system Hamiltonian matrix for the diagonalization is constructed with the adapted basis functions given as elite strings (characterized by high fitness scores) in the μ–GA population. Upon the selection of elite stings, we have considered not only the fitness scores but also the overlaps between the strings to avoid the numerical difficulties arising from the linear dependencies. Note that the Hamiltonian matrix elements are effectively evaluated by using Gaussian quadrature, since we adopt the Gaussian–type trial function

2.3 Water Trimer Model System

Now, we consider the application of the present method to the three–dimensional vibrational calculation of the water trimer. We employ the model Hamiltonian proposed by van der Avoird [15], in which the coordinates of the flipping motions are defined as angles between three free (non–hydrogen bonded) O–H bonds and O–O–O plane. The torsional angle space $\{\omega_1, \omega_2, \omega_3\}$ is defined as shown in Figure 2. The three hydrogen bonds in the WT are considered to be rigid. Thus, all the hydrogen bond lengths and internal angles are fixed except the three torsional angles stated above.

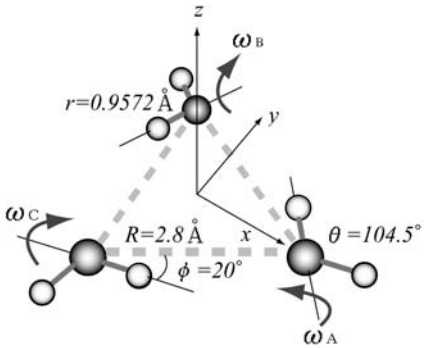

Figure 2. Definition of the free internal coordinates, 'torsional angles', of the water trimer.

The model Hamiltonian of the flipping motion of the WT is given as [12]:

$$\hat{H} = -\frac{\hbar^2}{2\Lambda} \sum_{\nu=A,B,C} \frac{\partial^2}{\partial \omega_\nu^{\,2}} + V(\omega_A, \omega_B, \omega_C) \tag{10}$$

where Λ denotes the effective moment of inertia, which is taken to be $\hbar^2/(2\Lambda) = 21.39\text{cm}^{-1}$ [12]. The potential function is analytically given in kcal/mol unit as

$$V(\omega_A,\omega_B,\omega_C)=\sum_{i<j}^{3}\left(\sum_{k\in i}^{7}\sum_{l\in j}^{7}332.0719\frac{z_k z_l}{r_{kl}}+\sum_{m\in i}^{4}\sum_{n\in j}^{4}a\exp\left[-br_{mn}\right]-cR_{ij}^{-6}\right) \tag{11}$$

which is called empirical potential using electrons and nuclei (EPEN) potential function. Subscripts *i*, *j* specify the water molecules consisting the trimer, whereas *k*, *l* denote effective point charge sites (for nuclei or electron pairs) and *m*, *n* indicate the sites for electron pairs [12].

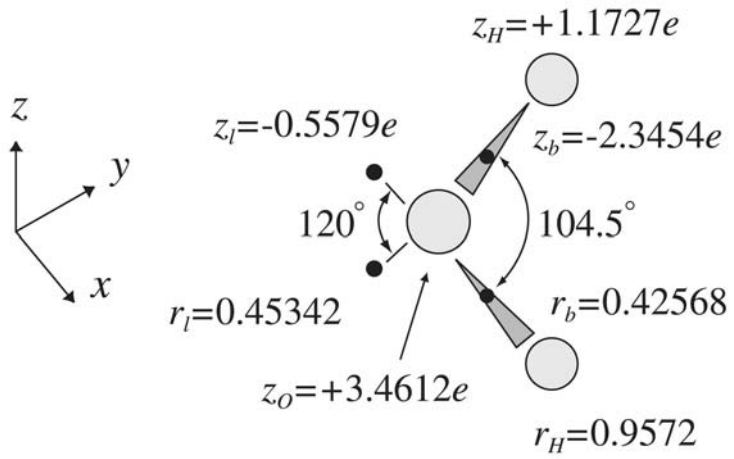

Figure 3. Positions of effective point charges for EPEN are shown as black dots. Unit length is angstrom (Å).

In Eq. (11), R_{ij} denotes the inter–nuclear distance between O_i and O_j and r_{kl} (r_{mn}) denotes the distance between the point charge sites *k* and *l* (*m* and *n*) on the water molecules *i* and *j*. The effective point charge z_k and the EPEN parameters *a*, *b*, and *c* are determined so as to reproduce the *ab initio* calculated energy surface. We adopt the parameters proposed by Bürgi *et al.*; *a* = 119.26 kcal/mol, *b* = 0.51793 Å and *c* = 3299 kcal/mol [12]. The EPEN has six global minima at around $\omega_\nu \cong \pm 50^\circ$. One of such minima corresponds to the structure with two H atoms above the O–O–O (O_3) plane (denoted as "up" = u) and one H below the O_3–plane (denoted as "down" = d), which we refer to (u,u,d). Then, other five structures corresponding to global minima are given as (u,d,d), (u,d,u), (d,d,u), (d,u,u), (d,u,d). We collectively denote these six structures as {uud}. Since the EPEN possesses S_6 symmetry, as shown above, we introduce symmetry adapted trial functions corresponding to the four irreducible representations of S_6, A_g, E_u, E_g and A_u, as follows.

$$\begin{aligned}\Psi_{A_g}(\omega_A,\omega_B,\omega_C)=\sum_{i=1}^{N}c_i\{&\exp\left[-a_{1i}(\omega_A+\omega_{1i})^2-a_{2i}(\omega_B-\omega_{2i})^2-a_{3i}(\omega_C-\omega_{3i})^2\right]\\&+\exp\left[-a_{1i}(\omega_A-\omega_{1i})^2-a_{2i}(\omega_B+\omega_{2i})^2-a_{3i}(\omega_C-\omega_{3i})^2\right]\\&+\exp\left[-a_{1i}(\omega_A-\omega_{1i})^2-a_{2i}(\omega_B-\omega_{2i})^2-a_{3i}(\omega_C+\omega_{3i})^2\right]\\&+\exp\left[-a_{1i}(\omega_A-\omega_{1i})^2-a_{2i}(\omega_B+\omega_{2i})^2-a_{3i}(\omega_C+\omega_{3i})^2\right]\\&+\exp\left[-a_{1i}(\omega_A+\omega_{1i})^2-a_{2i}(\omega_B-\omega_{2i})^2-a_{3i}(\omega_C+\omega_{3i})^2\right]\\&+\exp\left[-a_{1i}(\omega_A+\omega_{1i})^2-a_{2i}(\omega_B+\omega_{2i})^2-a_{3i}(\omega_C-\omega_{3i})^2\right]\}\end{aligned} \tag{12}$$

$$\begin{aligned}\Psi_{E_{u1}}(\omega_A,\omega_B,\omega_C) = \sum_{i=1}^{N} c_i \{ & 2\exp\left[-a_{1i}(\omega_A+\omega_{1i})^2 - a_{2i}(\omega_B-\omega_{2i})^2 - a_{3i}(\omega_C-\omega_{3i})^2\right] \\ & -\exp\left[-a_{1i}(\omega_A-\omega_{1i})^2 - a_{2i}(\omega_B+\omega_{2i})^2 - a_{3i}(\omega_C-\omega_{3i})^2\right] \\ & -\exp\left[-a_{1i}(\omega_A-\omega_{1i})^2 - a_{2i}(\omega_B-\omega_{2i})^2 - a_{3i}(\omega_C+\omega_{3i})^2\right] \\ & -2\exp\left[-a_{1i}(\omega_A-\omega_{1i})^2 - a_{2i}(\omega_B+\omega_{2i})^2 - a_{3i}(\omega_C+\omega_{3i})^2\right] \\ & +\exp\left[-a_{1i}(\omega_A+\omega_{1i})^2 - a_{2i}(\omega_B-\omega_{2i})^2 - a_{3i}(\omega_C+\omega_{3i})^2\right] \\ & +\exp\left[-a_{1i}(\omega_A+\omega_{1i})^2 - a_{2i}(\omega_B+\omega_{2i})^2 - a_{3i}(\omega_C-\omega_{3i})^2\right]\}\end{aligned} \tag{13}$$

$$\begin{aligned}\Psi_{E_{u2}}(\omega_A,\omega_B,\omega_C) = \sum_{i=1}^{N} c_i \{ & \exp\left[-a_{1i}(\omega_A-\omega_{1i})^2 - a_{2i}(\omega_B+\omega_{2i})^2 - a_{3i}(\omega_C-\omega_{3i})^2\right] \\ & -\exp\left[-a_{1i}(\omega_A-\omega_{1i})^2 - a_{2i}(\omega_B-\omega_{2i})^2 - a_{3i}(\omega_C+\omega_{3i})^2\right] \\ & -\exp\left[-a_{1i}(\omega_A+\omega_{1i})^2 - a_{2i}(\omega_B-\omega_{2i})^2 - a_{3i}(\omega_C+\omega_{3i})^2\right] \\ & +\exp\left[-a_{1i}(\omega_A+\omega_{1i})^2 - a_{2i}(\omega_B+\omega_{2i})^2 - a_{3i}(\omega_C-\omega_{3i})^2\right]\}\end{aligned} \tag{14}$$

$$\begin{aligned}\Psi_{E_{g1}}(\omega_A,\omega_B,\omega_C) = \sum_{i=1}^{N} c_i \{ & 2\exp\left[-a_{1i}(\omega_A+\omega_{1i})^2 - a_{2i}(\omega_B-\omega_{2i})^2 - a_{3i}(\omega_C-\omega_{3i})^2\right] \\ & -\exp\left[-a_{1i}(\omega_A-\omega_{1i})^2 - a_{2i}(\omega_B+\omega_{2i})^2 - a_{3i}(\omega_C-\omega_{3i})^2\right] \\ & -\exp\left[-a_{1i}(\omega_A-\omega_{1i})^2 - a_{2i}(\omega_B-\omega_{2i})^2 - a_{3i}(\omega_C+\omega_{3i})^2\right] \\ & +2\exp\left[-a_{1i}(\omega_A-\omega_{1i})^2 - a_{2i}(\omega_B+\omega_{2i})^2 - a_{3i}(\omega_C+\omega_{3i})^2\right] \\ & -\exp\left[-a_{1i}(\omega_A+\omega_{1i})^2 - a_{2i}(\omega_B-\omega_{2i})^2 - a_{3i}(\omega_C+\omega_{3i})^2\right] \\ & -\exp\left[-a_{1i}(\omega_A+\omega_{1i})^2 - a_{2i}(\omega_B+\omega_{2i})^2 - a_{3i}(\omega_C-\omega_{3i})^2\right]\end{aligned} \tag{15}$$

$$\begin{aligned}\Psi_{E_{g2}}(\omega_A,\omega_B,\omega_C) = \sum_{i=1}^{N} c_i \{ & \exp\left[-a_{1i}(\omega_A-\omega_{1i})^2 - a_{2i}(\omega_B+\omega_{2i})^2 - a_{3i}(\omega_C-\omega_{3i})^2\right] \\ & -\exp\left[-a_{1i}(\omega_A-\omega_{1i})^2 - a_{2i}(\omega_B-\omega_{2i})^2 - a_{3i}(\omega_C+\omega_{3i})^2\right] \\ & +\exp\left[-a_{1i}(\omega_A+\omega_{1i})^2 - a_{2i}(\omega_B-\omega_{2i})^2 - a_{3i}(\omega_C+\omega_{3i})^2\right] \\ & -\exp\left[-a_{1i}(\omega_A+\omega_{1i})^2 - a_{2i}(\omega_B+\omega_{2i})^2 - a_{3i}(\omega_C-\omega_{3i})^2\right]\end{aligned} \tag{16}$$

$$\begin{aligned}\Psi_{A_u}(\omega_A,\omega_B,\omega_C) = \sum_{i=1}^{N} c_i \{ & \exp\left[-a_{1i}(\omega_A+\omega_{1i})^2 - a_{2i}(\omega_B-\omega_{2i})^2 - a_{3i}(\omega_C-\omega_{3i})^2\right] \\ & +\exp\left[-a_{1i}(\omega_A-\omega_{1i})^2 - a_{2i}(\omega_B+\omega_{2i})^2 - a_{3i}(\omega_C-\omega_{3i})^2\right] \\ & +\exp\left[-a_{1i}(\omega_A-\omega_{1i})^2 - a_{2i}(\omega_B-\omega_{2i})^2 - a_{3i}(\omega_C+\omega_{3i})^2\right] \\ & -\exp\left[-a_{1i}(\omega_A-\omega_{1i})^2 - a_{2i}(\omega_B+\omega_{2i})^2 - a_{3i}(\omega_C+\omega_{3i})^2\right] \\ & -\exp\left[-a_{1i}(\omega_A+\omega_{1i})^2 - a_{2i}(\omega_B-\omega_{2i})^2 - a_{3i}(\omega_C+\omega_{3i})^2\right] \\ & -\exp\left[-a_{1i}(\omega_A+\omega_{1i})^2 - a_{2i}(\omega_B+\omega_{2i})^2 - a_{3i}(\omega_C-\omega_{3i})^2\right]\end{aligned} \tag{17}$$

We have carried out the hybrid–GA calculation for each irreducible representation with the population consisting of 80 strings up to 500 generations. The convergence check parameter ε for

the μ–GA breeding is taken to be 0.05. We use 3 Gaussians ($N = 3$ in Eq. (9)) to expand the trial function and the number of the random points used for the evaluation of $\tilde{f}$ are taken to be 6000.

3 RESULTS AND DISCUSSION

Listed in Table 1 are the eigenvalues and energy differences (in cm^{-1}) calculated by the μ–GA. Shown in GA+Var. columns are the refined values obtained by the final variational calculation. For the diagonalization, four elite strings are selected from the GA–populations bred with different random seeds. In order to avoid the numerical instability, we choose the elite strings whose mutual overlap integrals are not extremely close to unity. The values displayed in the 'difference' column indicate energy differences between the excited eigenstates and the A_g ground state.

Table 1. Eigenvalues and Energy Differences (cm^{-1}) of the Water Trimer Calculated by μ–GA

	GA eigenvalue	GA+Var. eigenvalue	GA difference	GA+Var. difference	DVR [9] difference
A_u	–231.56	–233.24	63.79	57.32	61.35
E_g	–248.76	–245.47	46.59	45.08	43.26
	–247.83	–245.84	47.52	44.70	43.26
E_u	–274.08	–278.13	21.27	12.41	13.63
	–274.73	–277.86	20.62	12.68	13.63
A_g	–295.35	–290.54	0.00	0.00	0.00

The energy differences calculated by DVR method with $15 \times 15 \times 15$ basis functions are shown together in the Table 1 for comparison [9]. Most of the calculated values are in good agreement with the results of the Blume's DVR calculation except the ones corresponding to E_u state. Since the μ–GA results contain the stochastic errors, it is considered that the calculated eigenvalues of E_u states have not been converged enough to the exact values. These discrepancies in the results of E_u states are corrected by the post–optimization, i.e., the variational calculation. The results shown in Table 1 seem to contradict the variational principle, that is, some eigenvalues refined by the variational calculation take larger values than the ones obtained by the μ–GA search. This can be explained by the fact that the eigenvalues sought by μ–GA do not necessarily correspond to the expectation values of the system Hamiltonian $\langle \hat{H} \rangle$, since the eigenvalue E is optimized independently in the μ–GA breeding process. It is confirmed that the Hamiltonian expectation value $\langle \hat{H} \rangle$ decreases through the final variational calculation in all cases.

Shown in Figure 4 is the fitness profile of the μ–GA calculation for A_g state. As is well–acknowledged, the convergence efficiency in the early generations is excellent. The abrupt jump on the profile at around the 400^{th} generation corresponds to the fact that the GA–population escapes from one of the local minima in the search space.

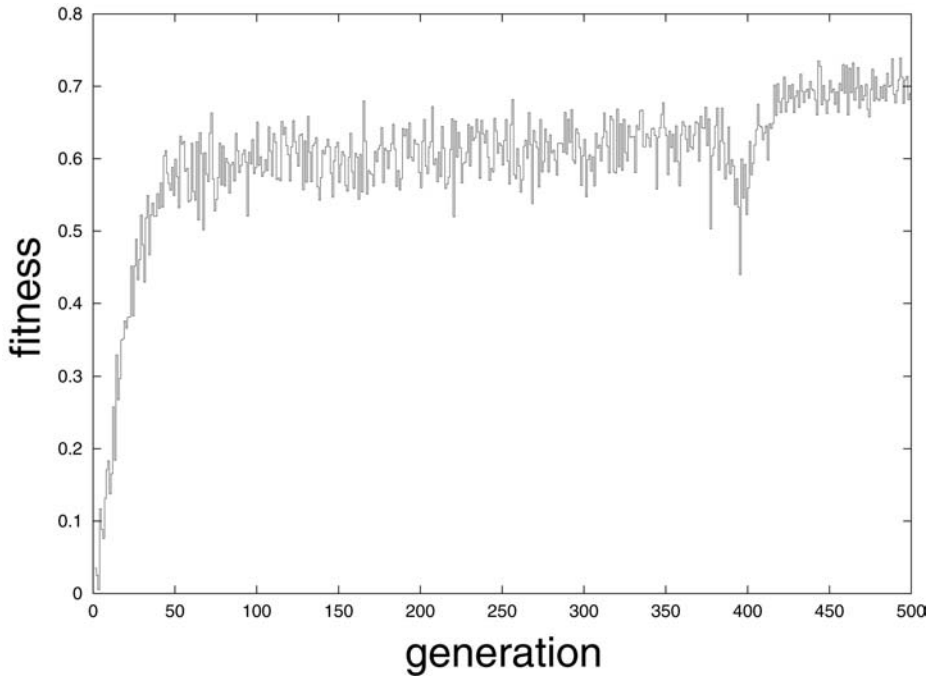

Figure 4. Fitness profile of the GA–breeding process in the calculation of A_g state.

Shown in Figure 5(a) is the eigenfunction of A_g state drawn as a function of ω_A and ω_C by fixing ω_B to 48°, while its contour plot is shown in Figure 5(b). Three peaks in the Figure 5 at around $\pm 48^\circ$ correspond to the global potential minima, (u,u,d), (d,u,d), and (d,u,d) structures.

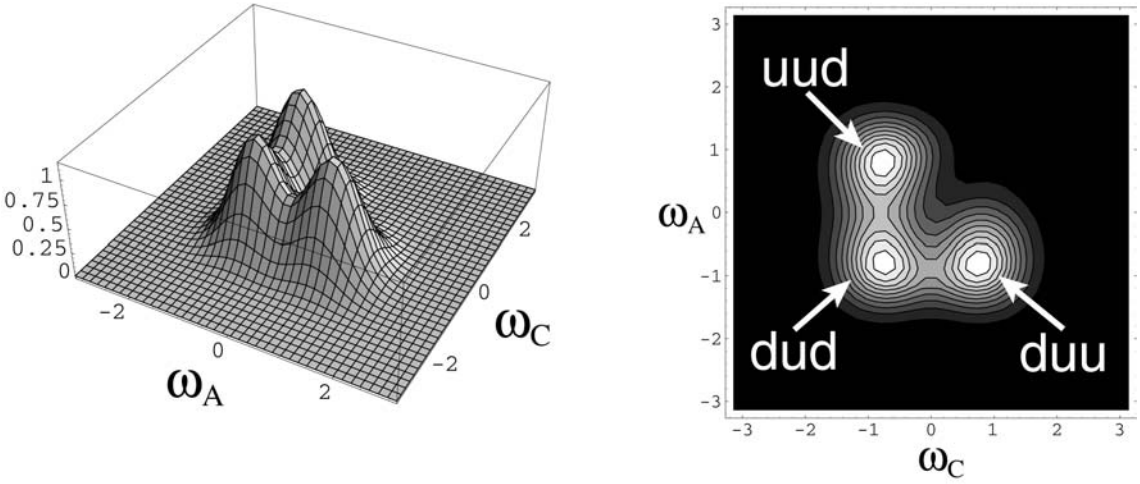

Figure 5. (a) 3D–plot of the eigenfunction of the A_g state. (b) Contour–plot of the eigenfunction of the A_g state.

For comparison, we have carried out the μ–GA calculation with the deterministic fitness score f defined as Eq. (7). The integrations that appear in f are evaluated numerically by introducing three–dimensional grid. The μ–GA calculation carried out with f evaluated by 8000 grid points fails to produce satisfactory results since the population is trapped in the local minima of the search space. On the other hand, the calculation with the stochastic fitness $\tilde{f}$ evaluated by 6000 sampling points

gives the appropriate results shown above. Thus, it is found that the stochastic fitness is quite an efficient fitness evaluation approach which works fine together with the μ–GA [18]. Finally, we introduce the self–correlation function in order to estimate the tunneling time from the energy differences in the Table 1. Consider that the wave function of the WT is initially localized in one of the 3–D potential wells, which is expressed as ket $|\varphi\rangle$. Since $|\varphi\rangle$ is the wave packet, or the linear combination of the eigenfunctions of WT (as shown in the following equation), it evolves as

$$\begin{aligned}
|\varphi(t)\rangle &= \exp[\frac{-i\hat{H}t}{\hbar}]|\varphi\rangle \\
&= \exp[\frac{-i\hat{H}t}{\hbar}]\left(|\Psi_{A_g}\rangle + |\Psi^{(1)}_{E_u}\rangle + |\Psi^{(2)}_{E_u}\rangle + |\Psi^{(1)}_{E_g}\rangle + |\Psi^{(2)}_{E_g}\rangle + |\Psi_{A_u}\rangle\right) \\
&= \exp[\frac{-iE_{A_g}t}{\hbar}]|\Psi_{A_g}\rangle + \exp[\frac{-iE_{E_u}t}{\hbar}]|\Psi^{(1)}_{E_u}\rangle + \exp[\frac{-iE_{E_u}t}{\hbar}]|\Psi^{(2)}_{E_u}\rangle \\
&+ \exp[\frac{-iE_{E_g}t}{\hbar}]|\Psi^{(1)}_{E_g}\rangle + \exp[\frac{-iE_{E_g}t}{\hbar}]|\Psi^{(2)}_{E_g}\rangle + \exp[\frac{-iE_{A_u}t}{\hbar}]|\Psi_{A_u}\rangle
\end{aligned} \tag{18}$$

Here, we define the self–correlation function as $\langle\varphi|\varphi(t)\rangle$. Then, the returning probability to the initial state $|\varphi\rangle$ at $t = t$, $P(t)$, is given as $P(t) = |\langle\varphi|\varphi(t)\rangle|^2$. By using the obtained eigenvalues, $P(t)$ can be readily calculated through Eq. (18). Shown in Fig. 6 is the time–dependence of $P(t)$. It is seen that partial recurrences due to the tunneling effects occur frequently. However, to achieve the complete recurrence, that is, $P(t) = 1$, one needs to await about 1200ps (= 1.2 ns), which can be considered as the overall tunneling time of the flipping motion of WT.

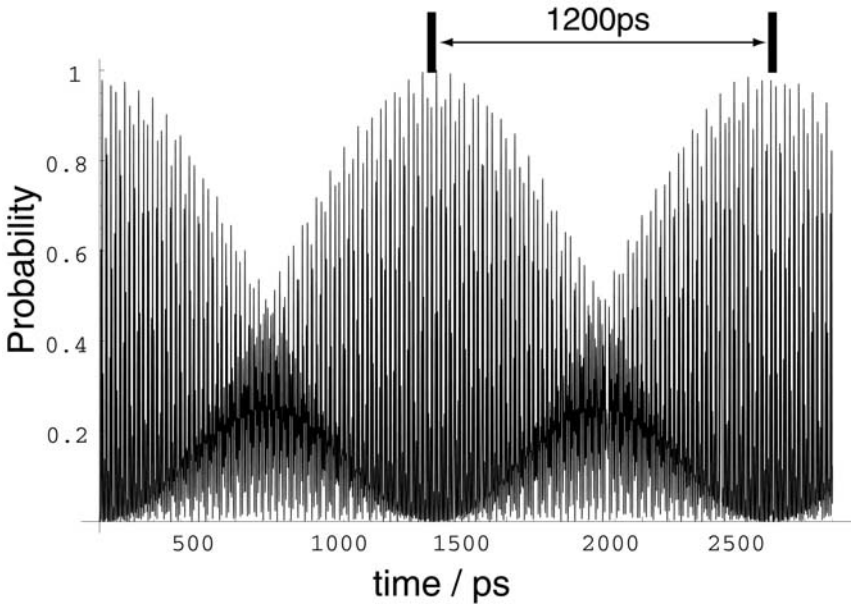

Figure 6. Time–dependence of the returning probability with respect to the flipping motion of WT.

4 CONCLUSIONS

We have calculated the vibrational eigenfunctions with respect to "flipping motion" of the water trimer. In order to solve the three–dimensional Schrödinger equation, we employed the hybrid μ–GA method together with the stochastically defined fitness score. To overcome the GA's slow convergence to the exact solution in the final stage, we utilized the variational calculation using the elite strings bred by the μ–GA. The trial functions were expanded in the three–dimensional symmetry adapted Gaussian functions, with which one can readily evaluate the Hamiltonian matrix elements. By adopting the stochastic fitness evaluation, we have largely reduced the actual computation, which makes it possible to carry out the multi–dimensional calculation effectively. Although we employed the variational calculation as a final optimizer in this study, there exist other possibilities in the choice of deterministic optimizer, such as steepest descent method, which was used in our previous work [18].

Finally, it should be stressed here that the μ–GA's future potential applicability to the multi–dimensional quantum mechanical calculation is promising. This is because GA is an intrinsically parallel algorithm and the GA–related computation can be efficiently distributed over several workstations/personal computers.

Acknowledgment

This work was supported, in part, by Research and Development Applying Advanced Computational Science and Technology, Japan Science and Technology Corporation, and by a Grant–in–Aid for Scientific Research from Ministry of Education, Science, Culture, and Sports of Japan. Authors are grateful to Dr. D. L. Carroll for his Fortran GA driver, which is open to the public through the Internet.

5 REFERENCES

[1] D. J. Wales, Structure, Dynamics, and Thermodynamics of Clusters: Tales from Topographic Potential Surfaces, *Science* **1996**, *271*, 925–929.
[2] D. J. Wales, Theoretical Study of Water Trimer, *J. Am. Chem. Soc.* **1993**, *115*, 11180–11190.
[3] M. Schutz, T. Burgi, S. Leutwyler, and H. B. Burgi, Fluxionality and Low–Lying Transition Structures of the Water Trimer, *J. Chem. Phys.* **1993**, *99*, 5228–5238.
[4] W. Klopper, M. Schutz, H. P. Luthi, and S. Leutwyler, An Ab–Initio Derived Torsional Potential–Energy Surface for $(H_2O)_3$. II. Benchmark Studies and Interaction Energies, *J. Chem. Phys.* **1995**, *103*, 1085–1098.
[5] W. Klopper, M. Schutz, 2–Dimensional Model Treatment of Torsional Motions the Water Trimer, *Chem. Phys.* Lett. **1995**, *237*, 536–544.
[6] J. K. Gregory and D. C. Clary, Calculations of the Tunneling Splittings in Water Dimer and Trimer Using Diffusion Monte–Carlo, *J. Chem. Phys.* **1995**, *102*, 7817–7829.
[7] J. K. Gregory and D. C. Clary, 3–Body Effects on Molecular–Properties in the Water Trimer, *J. Chem. Phys.* **1995**, *103*, 8924–8930.
[8] J. E. Fowler and H. F. Schaefer III, Detailed Study of the Water Trimer Potential–Energy Surface. *J. Am. Chem. Soc.* **1995**, *117*, 446–452.
[9] D. Sabo, Z. Bacic, T. Burgi, and S. Leutwyler, 3–Dimensional Model Calculation of Torsional Levels of $(H_2O)_3$ and $(D_2O)_3$. *Chem. Phys. Lett.* **1995**, *244*, 283–294.
[10] D. Sabo, Z. Bacic, S. Graf, and S. Leutwyler, Four–dimensional Model Calculation of Torsional Levels of Cyclic Water Tetramer, *J. Chem. Phys.* **1998**, 109, 5404–5419.
[11] D. Blume and K. B. Whaley, Tunneling Splittings in Water Trimer by Projector Monte Carlo, *J. Chem. Phys.* **2000**, *112*, 2218–2226.

[12] T. Burgi, S. Graf, S. Leutwyler, and W. Klopper, An Ab–Initio Derived Torsional Potential–Energy Surface for $(H_2O)_3$. I. Analytical Representation and Stationary–Points, *J. Chem. Phys.* **1995**, *103*, 1077–1084.
[13] N. Pugliano and R. J. Saykally, Measurement of Quantum Tunneling between Chiral Isomers of the Cyclic Water Trimer, *Science* **1992**, *257*, 1937–1940.
[14] K. Liu, M. J. Elrod, J. G. Loeser, J. D. Cruzan, N. Pugliano, M. G. Brown, J. Rzepiela, and R. J. Saykally, Far–Ir Vibration–Rotation Tunneling Spectroscopy of the Water Trimer, Faraday Discuss. Chem. Soc. **1994**, *35*, 35–41.
[15] van der Avoird, E. H. T. Olthof, and P. E. S. Wormer, Tunneling Dynamics, Symmetry, and Far–infrared Spectrum of the Rotating Water Trimer. I. Hamiltonian and Qualitative Model. *J. Chem. Phys.* **1996**, *105*, 8034–8050.
[16] S. Suzuki and G. A. Blake, Pseudorotation in the D_2O Trimer. *Chem. Phys. Lett.* **1994**, *229*, 499–505.
[17] D. L. Carroll, Genetic Algorithms and Optimizing Chemical Oxygen–Iodine Lasers, in: *Developments in Theoretical and Applied Mechanics Vol. XVIII*, *Eds*. H. Wilson, R. Batra, C. Bert, A. Davis, R. Schapery, D. Stewart, F. Swinson, School of Engineering, The University of Alabama, 1996, pp 411–424.
[18] M. Sugawara, Numerical Solution of the Schrödinger Equation by Neural Network and Genetic Algorithm, *Comput. Phys. Comm.* **2001**, *140*, 366–380.

Biographies

Michihiko Sugawara is assistant professor of theoretical chemistry at the Department of Chemistry, Faculty of Science and Technology, Keio University, Japan.

Hiromi Nakanishi is currently working for Shiseido Inc, and was a graduate student at the Department of Chemistry, Faculty of Science and Technology, Keio University, Japan.

Satoshi Yabushita is professor of quantum chemistry at the Department of Chemistry, Faculty of Science and Technology, Keio University, Japan.